Cryst. Res. Technol. **40**, No. 9, 905 – 916 (2005) / **DOI** 10.1002/crat.200410456

Microstructure of a genuine Damascus sabre

A. A. Levin[1], D. C. Meyer[1], M. Reibold[1], W. Kochmann[2], N. Pätzke[1], and P. Paufler*[1]

[1] Institut für Strukturphysik, TU Dresden, D-01062 Dresden, Germany
[2] Krüllsstrasse 4b, 06766 Wolfen, Germany

Received 11 November 2004, accepted 24 January 2005
Published online 15 August 2005

Key words Damascene steel, X-ray phase and texture analysis, HRTEM analysis.
PACS 61.10, 61.14.-x, 81.07.De

The surface and cross-section of a genuine Damascus sword was characterised by means of wide-angle X-ray scattering techniques complemented by optical and transmisssion electron microscopy. Position-resolved X-ray phase analysis revealed that, unlike ferrite and martensite, the distribution of cementite is inhomogeneous in different spatial zones parallel to the cutting edge of the blade. For the first time a quantitative X-ray phase and texture analysis was made possible by averaging all spatial zones of the surface and the cross-section of the sword and applying the Rietveld method with code TOPAS. Differences concerning texture and structure characteristics of ferrite, martensite and cementite are discussed. More evidence for the structure of cementite nanowires is supplied.

1 Introduction

A number of papers and books have been published on the fascinating legends and excellent properties of Damascene blades (see, for more recent examples, Refs. [1-5]). Genuine or wootz Damascus blades, known in Russia as 'bulat', were manufactured in medieval Damascus from so-called 'wootz' steel which in turn was made in India and characterised by a typical impurity content. Damascene swords, sabres and daggers became famous for their hardness, retention of their cutting edge, mysterious secrets of the forging, quenching and annealing procedures and a beautiful characteristic pattern of light-coloured wavy fine bands over the grey background of steel. The museum-quality wootz Damascus blades were produced mainly in 16th –17th centuries. In the early 19th century, the last secrets of the genuine Damascus steel got finally lost, but since that time several attempts have been performed to rediscover the recipes of achieving blades of comparable quality (cf. [6-13, 55]). Applying optical microscopy to polished blades, Belaiew identified the beautiful watering as 'milky ways' of cementite (Fe_3C) and concluded that small, round-shaped cementite is embedded in the ground-mass of damascene steel thus avoiding the typical brittleness of hypereutectoid steels with their needle-form cementite [9]. The spheroidisation seemed to be the consequence of repeated hammering and heating. The cementite veins run closer up to the edge of the blade thus providing good cutting properties. Belaiew supposed that the properties and the distribution of the carbides play a more considerable role than the (martensitic) matrix. Harnecker [13] offered experimental evidence that forging at temperatures below the temperature of cementite formation from austenite, A_{cm} ($A_{cm} \approx 850°C$), leads to the destruction of needle-like cementite and, after heat treatment, to spheroidization of Fe_3C. According to [10], whilst being very strict as regards the forging temperature, insufficient attention had been paid to the subsequent heat treatments at that time. Annealing above A_{cm} would make the cementite disappear and the exceptional properties of the steel get lost.

Though being precious samples of various collections, some genuine Damascus blades including occasionally broken pieces have been subjected to a more thorough metallographic investigation accepting their destruction. Zschokke [12] was seemingly the first who reported on an analysis of definite blades donated by Henri Moser to the Historic Museum Berne (see also [14]). Later on, other authors contributed their results (e.g. [15] – [19]) utilising 20th century's analytic tools. Belaiew's finding that both shape, size and distribution of cementite was the characteristic feature of Damascus blades has not only been confirmed but also elucidated at a microscopic scale.

* Corresponding author: e-mail: paufler@physik.tu-dresden.de

It is generally agreed that the beautiful patterns arise from the aggregation of carbide particles. The processing steps and the physical mechanisms behind them, however, remain a subject of debate still today. Comparing metallographic data of these blades with alloys synthesised to reproduce genuine Damascus material, various models have been proposed. Wadsworth et al. [2] assumed that the major process route was heating the steel above the temperature, A_{cm} , to form large austenite grains, then cooling slowly to form cementite on the austenite grain boundaries and breaking up and spreading out of cementite by subsequent forging. Verhoeven et al. [16], and Verhoeven [5], however, observed the dissolution of the original Damascus cementite distribution after heating to ~925°C for 30 min and subsequent slow cooling, what let them conclude that first only part of the cementite is formed by cooling the blade to around 50K below A_{cm} and breaking up the much thinner array of cementite in the first forging steps. Then the remaining fraction of equilibrium cementite is forced to precipitate on the broken-up cementite by holding the temperature around 50-100K below A_{cm} for the first forging steps and then cooling slowly to temperatures around 750-800 °C for final forging. Recrystallisation of the austenite (i.e. formation of new grain boundaries) has to be avoided by keeping the amount of plastic deformation small. Wadsworth et al. [21] pointed out that the results of [16] seem to refer to a blade which was not a genuine one. Apparently controversial results might reflect different paths of processing [21].

Also, the role of minor amounts of alloying elements other than carbon upon the formation of cementite cluster sheets has to be taken into account. Small additions of Mn, Si, P, and S seem to enhance the breakup of cementite into spherodized agglomerates [18]. Later on, Verhoeven et al. [22,23] and Verhoeven [5] proposed that the carbide-forming metals V, Cr, Ti, Mo, Nb, and Mn, present at individual levels of 20-to-100 ppmw and micro-seggregated in interdendritic regions, facilitate the formation of cementite bands during the thermal cycling done at temperatures below A_{cm}. Studies of the effect of Si and V upon the mechanical properties of modern pearlitic steels have shown that V increases the strength of pearlite, mainly by precipitation strengthening of ferrite, whereas Si strengthens pearlite by solid-solution hardening of ferrite. The ductility in hypereutectoid steels is increased by V and Si [49]. Verhoeven [5] presumed that the lack of a certain level of impurities in the Indian wootz manufactured since the beginning of the 19th century might have been the reason for the decline of Damascus blade production at this time.

It is well known that steel of a carbon content between 1 and 2 wt.%, after casting, produces a microstructure with massive plates of cementite, giving rise to high hardness but low ductility. The question how mediaeval blacksmiths could overcome this detrimental brittleness has been answered by Sherby et al. [24] and Wadsworth [21]. They demonstrated that, by mechanical processing at suitable temperatures, this microstructure can be converted into a very fine-grained structure which in turn is superplastic, i.e. not brittle any more.

A new view upon the microstructure and the properties of Damascus steel has been opened by the finding of Kochmann et al. [25]. Using high-resolution transmission electron microscopy (HRTEM), they detected a high density of cementite nanowires (diameter 10-20 nm, lengths several hundred nm) in a genuine Damascus sabre. These components of the microstructure at nanometer scale have certainly been overlooked so far because of the resolution needed. Kochmann et al. [25] reported on preliminary results concerning structural data. The present work is aimed at communicating results of a thorough analysis of X-ray data referring to the Damascus sabre of ref. [25] complemented by optical micrographs and electron microscopy. Due to heterogeneity and severe texture of the manufactured swords, the X-ray diffraction investigation is usually restricted to a qualitative X-ray phase analysis [55]. In the present work we succeeded for the first time in a quantitative X-ray phase and texture analysis by averaging all spatial zones of the surface and the cross-section of the blade applying the Rietveld method with code TOPAS. The influence of annealing upon the microstructure and results of hardness measurements will be dealt with elsewhere [33].

2 Experimental

2.1 Specimen and microstructure

The specimen used in the present investigation is a part of the genuine Damascus sabre produced by the famous blacksmith Assad Ullah in the 17th century (cf. [12, 14]). In the first metallographic investigation [12] of various blades from the Berne museum, the present sabre was labelled No. 10 and rated as a sword with the most beautiful Damascus pattern. E. J. Kläy (Berne Historical Museum, Switzerland) provided individual pieces of that sabre No. 10, containing the cutting edge, for further investigation to J. D. Verhoeven (cf. [22],

there termed ‘sword No. 10’), to J. Piaskowski [15] and to one of us (W.K.) [25, 26]. The specimen of the report [25] was used for the present investigation, too.

From one side of the specimen available, several pieces were cut off by a diamond wire saw to study the cross-section of the blade. Micrographs of the specimens used for X-ray diffraction measurements have been obtained by optical microscopy (Figs. 1, 2 and 3). Fig. 1 shows the famous Damascene surface pattern, which is due to banding of cementite grains. These particles appear as layers of bright areas in the cross-section of the blade (Figs. 2-3).

First, wide-angle X-ray scattering (WAXS) patterns were recorded from the surface of the sabre (left piece of Fig. 1, surface size of 16 mm x 18 mm). The cross-section specimen (right part of Fig. 1, rotated at an angle of 90° to the left (former host) piece) utilised for X-ray investigation of the interior structure of the sabre exhibited an isosceles curved-side triangle form (base of ~3 mm and height of ~16 mm, thickness of about 2 mm). The division of the sample was necessary in order to study the phase content of the interior of the sample. With the X-ray radiation used only layers with a thickness of the order of magnitude of 10 μm could be subjected to an X-ray phase analysis.

Most important parameters of the microstructure of genuine Damascus blades are the spacing of the characterisitic cementite bands and the diameter of the spheroidised cementite. Our data (L) compare favourably with those of Zschokke [12] (Z): Band spacing 40-60 μm (L), 30-50 μm (Z); cementite particle diameter 1-10 (L) , 10 (Z).

Fig. 1 Surface (left) prior to metallographic treatment and cross section (right) of the piece of the Damascus sabre investigated. The light spot on the surface is due to etching. Scale is in cm.

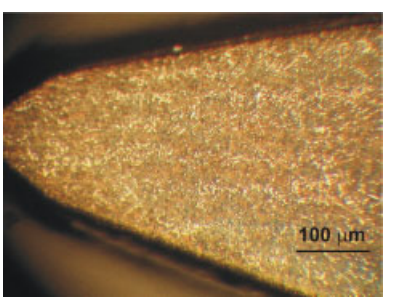

Fig. 2 Cross-section specimen of Fig. 1 ground with SiC paper grades 1000, 2400, and 4000, respectively; polished using diamond suspension 3 μm, etched in 1.5% alcoholic nitric acid. The horizontal banding of cementite particles (bright phase) with a spacing of ~50- 60 μm is clearly visible. Cutting edge of the sabre on the left hand side.

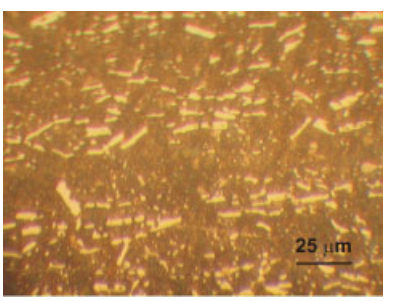

Fig. 3 Micrograph of the cross-section specimen of Fig. 1 at higher magnification. The cementite particles appear as bright small equiaxed and larger oblong areas. Photograph taken 2 mm off the cutting edge (left hand).

2.2 Elemental analysis

The average composition and distribution of non-iron elements has been determined in a previous work [25] by optical emission spectrometry. For the sake of comparison, results of independent analyses of the same sabre (but different places along the blade) are provided in Tab. 1. Apart from these elements, traces of Pb, Sn, Ca, Ce, B [25] and, additionally, Ti, and Zr [19] have also been detected in amounts far below the estimated uncertainty (0.08 wt. % for C and 0.01 wt. % for the rest). In addition, with the aid of energy dispersive X-ray analysis and electron energy loss spectrometry, small quantities of Ce , Nd , Sm, Th and Ce have been observed near the area prepared for transmission electron microscopy. With the exception of C, the agreement with [12] and [19] is good. Presumably, the differences are rather reflecting compositional gradients than different uncertainties of measurement. This is supported by electron scanning microanalysis and EDX analysis, which revealed composition gradients along the sabre. The presence of rare earths may be a fingerprint of the source of wootz steel used [25].

Table 1 Composition (wt.%) of a Damascus blade (labelled No.10 in [12]).

Authors, Sword label	C	Mn	P	S	Si	Ni	Co	Cr	Cu	V	Mo	W	Nb	Al
Zschokke [12], Plate VII, No. 10	1.726	0.028	0.172	0.020	0.062									
Verhoeven et al. [19], Zschokke No. 10	1.79	0.03	0.13	0.016	0.05	0.07		<0.01	0.18	0.027	<< 0.01		<0.01	0.01
Kochmann et al. [25], Zschokke No. 10	2.24	0.02	0.11	0.04	0.04	0.05	0.05	<0.01	0.17	0.02	<0.01	<0.01	<0.01	0.05

2.3 X-ray diffraction

Both specimens were investigated by means of WAXS using two modifications of the method. To determine the phase composition of the different areas of the specimens, X-ray diffraction patterns were recorded of 7 spatial zones of the specimen starting from the cutting edge up to the back. These zones of width of about 2 mm were selected by appropriate exposure by X-rays using slits of corresponding width. During the spatially resolved measurements, no specimen rotation around the surface normal was performed. The measurements were carried out using an X-ray diffractometer HZG-4 (Seifert FPM GmbH, Germany) with a Cu tube with fine focus of about 0.04 mm width. A primary Si(111) monochromator tuned to CuK_β radiation and a scintillation detector were used. Measurements were carried out applying the symmetrically coupled $\theta/2\theta$ scan mode (where θ is the angle of incidence of X-rays and 2θ is the detection angle) in the wide-angle 2θ range from 7.5° to 120° with a step width of 0.05° (2θ) and a sampling time of 10 s per angle step. To reduce statistical fluctuations of the recorded intensities, multiple scan and summing up of the individual intensity data-sets was performed. Hence the total sampling time per angle step was 130 s for the big piece representing the surface of the sword and 200 s for the smaller cross-section specimen, respectively.

A similar technique was applied to obtain the X-ray diffraction patterns for spatially averaging quantitative analysis. Measurements were performed in the symmetrically coupled $\theta/2\theta$ scan mode using an X-ray diffractometer URD-6 (Seifert FPM GmbH, Germany) in Bragg-Brentano geometry. CuK_α radiation monochromatised by a secondary graphite monochromator and recorded by a scintillation detector was used. In order to minimise influences of preferred orientation (texture) effects, the specimen was rotated around the holder axis during the measurements. The central area of the specimen of about 10 mm in diameter was exposed by X-rays. Multiple scans of the 2θ range from 15° to 120 ° (for the 'surface blade' specimen) and from 24.5° to 120° (cross-section specimen) were carried out with a 2θ step width of 0.02° and 10 s sampling time per angle step. The total sampling time per angle step after summing up the individual scan intensity data-sets was 110 s and 150 s, respectively.

To control the alignment and calibration of the diffractometer, the X-ray diffraction patterns of the specimens were recorded under addition of a thin silicon cover layer (Standard Reference Material 640b of NIST). The data obtained this way were used as an external standard for refinement of the unit cell parameters of the specimen specific crystalline phases.

2.4 Quantitative phase analysis

The quantitative analysis was carried out by fitting the complete X-ray diffraction patterns (CuK_α radiation) according to a Rietveld structure refinement procedure using the computer programme TOPAS 2.0 [27]. The initial structure models of the compounds used for the refinement of parameters of phases contained in the specimen and identified by comparison with the Powder Diffraction File (PDF) (α-Fe ferrite, Fe_3C cementite, Fe-C martensite and graphite) were taken from [28]. Crystallographic data of these phases are shown in Tab. 2. The atomic coordinates and occupancy factors of atomic positions were not refined. Refinement was carried out using a general temperature factor for all atoms of the structure model. Scattering factors of neutral atoms [29] and a pseudo-Voigt function [30] for fitting the reflection profiles were used.

Comparison of experimental and calculated X-ray diffraction patterns of the Fe-C phases found in the specimen revealed a great influence of texture. The refinement procedure without application of the texture resulted in poor fitting of a number of reflections. In any case the intensities exceeded the calculated ones. The texture of the phases contained in the specimens was taken into account by a March-Dollase model [30,31]. The direction of the preferred orientation was determined by trial fittings taking the reflection indices of the otherwise poorly fitted profiles as preferred orientation directions.

At the final stages of the refinement, the size of crystallites of the phases observed was estimated using the programme TOPAS based on the 'Scherrer equation' [30]. All estimated standard deviations (e.s.d.) obtained

by a Rietveld least-square refinement were multiplied by a factor calculated with the aid of a computer programme estimating probable errors of Rietveld refinement with serial correlation by a procedure decribed in [32]. The structural parameters exhibiting high e.s.d. values in the first cycles of refinement were fixed during the next stages of refinement.

2.5 Electron microscopy

Thin foils were prepared for HRTEM parallel and perpendicular to the surface of the blade by a standard technique involving mechanical grinding, mechanical dimpling and ion milling to perforation. The samples were examined in a Philips CM200 FEG microscope operated at 200 kV to identify the real structure at an atomic level.

3 Results and discussion

3.1 Position-resolved X-ray phase analysis

X-ray diffraction patterns recorded from sequential zones of ~2 mm width, spatially neighboured and oriented parallel to the cutting edge of the blade, are shown in Figs. 4 and 5 for both, surface and cross-section pieces of the sword, respectively.

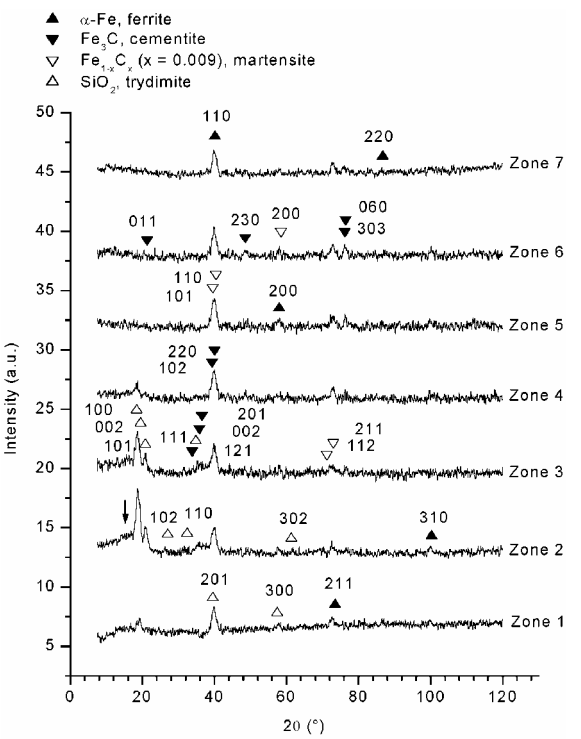

Fig. 4 Intensity versus diffraction angle 2θ measured in the symmetrically coupled θ/2θ scan mode (CuK_β radiation). Zone 1 through 7 represent sequentially neighboured positions of the primary X-ray beam along the surface of the blade, oriented parallel to the cutting edge. The numbering of the zones starts from the cutting edge of the blade. The width of zones was about 2 mm. X-ray diffraction patterns obtained for different zones are shifted vertically to facilitate visual inspection. Reflection indices are given for the corresponding reflection positions which are indicated by triangles. These positions were calculated for the structures indicated at the top using structural data of [28]. An arrow (Zone 2) marks a wide shoulder arising probably from an unknown phase.

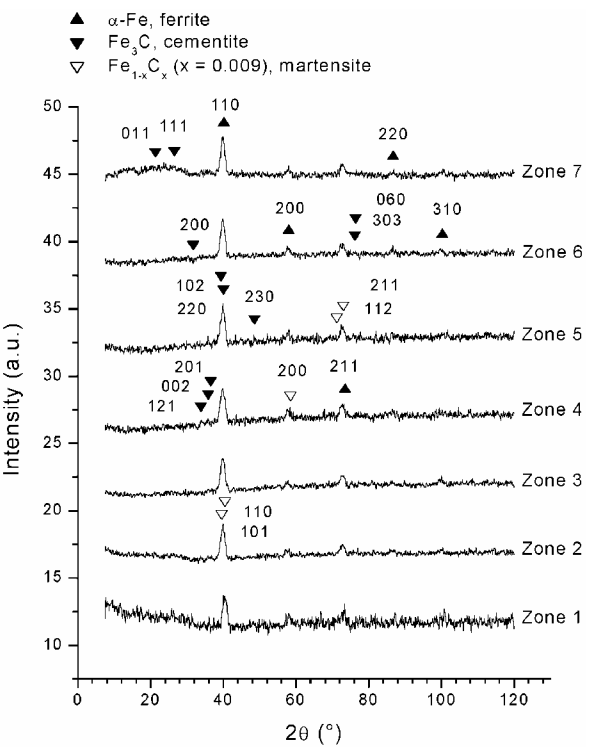

Fig. 5 Intensity versus diffraction angle 2θ measured in the symmetrically coupled θ/2θ scan mode (CuK_β radiation) obtained from the cross section of the blade. Zone 1 through 7 represent sequentially neighboured positions of the primary X-ray beam along the cross section, oriented parallel to the base line of the isosceles triangle (see Fig.1). The numbering of the zones starts from the cutting edge of the blade. The width of zones was about 2 mm. X-ray diffraction patterns obtained for different zones are shifted vertically to facilitate visual inspection. Reflection indices are given for the corresponding reflection positions which are indicated by triangles. These positions were calculated for the structures indicated at the top using structural data of [28].

The zones of the surface screened exhibited different phase content as to be seen already by visual inspection of Fig. 4, whereas the changes are less pronounced in Fig. 5. The latter is in agreement with the orientation of cementite-banding displayed in Fig. 2a.

Reflections of ferrite (α-Fe, Tab. 2) are observed in all zones starting from the cutting edge. They seem to be overlapped by reflections from tetragonally distorted $Fe_{1-x}C_x$ martensite (Tab. 2). Examples of the well-resolved fine structure of the experimental reflection profiles are presented in insets of Fig. 6 for the most intensive ferrite reflection recorded with CuK_α radiation and a smaller 2θ angle step width of 0.02°. Contrary to ferrite and martensite, the distribution of Fe_3C cementite was found to be inhomogeneous in agreement with Figs. 2, 3 and [25]. Cementite reflections were detected firstly in zone 3 (Fig. 4) about 6 mm away from the cutting edge reaching the maximum intensities in zones 5 and 6 (back of the blade). Apparently, due to preferred orientation effects, the most intensive reflection referred to cementite is a result of overlapping of two Fe_3C reflections with close spacings and reflection indices 060 and 303. No indications of austenite were found in any zone neither in surface nor in cross-section samples of the sword.

Table 2 Structural data adopted from [28].

Crystalline phase	Structure type [a]	*a* (Å)	*b* (Å)	*c* (Å)
α–Fe (ferrite)	(229) $Im\bar{3}m$ - *a*, cI2 (W type)	2.8665	*a*	*a*
Fe_3C (cementite)	(62) Pnma - dc^2, oP16 (Fe_3C type)	5.0890	6.7433	4.5235
$Fe_{20}C$ (martensite)	(139) *I*4/*mmm* – *ba*, tI4 (Martensite type)	2.854 [c]	*a*	2.985 [c]
C (graphite)	(194) $P6_3/mmc$ – *ba*, hP4 (Graphite type)	2.464 [b]	*a*	6.711 [b]

[a] (Number of space group) space group symbol – Wyckoff letters of atomic positions, Pearson symbol (old notation of the structure type)
[b] From other literature sources [28], *a* = 2.47 Å, *c* = 6.93 Å for graphite
[c] *a* = 2.845 Å, *c* = 2.970 Å for $Fe_{1-x}C_x$, x = 0.009 (see [34], p. 491)

In the areas near the cutting edge of the blades (zones 1 – 4 in Fig. 4), the reflections referred to the hexagonal modification of SiO_2, trydimite, (*a* = 5.010 Å, *c* = 8.180 Å, space group $P6_322$ [35]) were found. Seemingly, a wide shoulder at 2θ ≈ 18.5°, marked by an arrow in Fig. 4, represents an unknown phase which could not be identified so far due to the limited data available. Reflections attributed to trydimite and this unknown phase were found in the patterns recorded from the zones near the cutting edge of the blade surface exclusively. Probably, the existence of these crystalline phases near the blade's surface is connected with pecularities of processing the surface of the cutting edge (inclusive later grinding).

Contrary to the surface of the sword, the X-ray pattern of the cross-section (Fig. 5) exhibited mainly the ferrite as well as the martensite reflections in all spatial zones. There are no distinct reflections attributed exclusively to Fe_3C, although the enhanced intensities at angle-positions of Fe_3C reflections indicate the existence of cementite. Since the cross-section was scanned along a direction parallel to the cementite layers the phase content of cementite did not change significantly in accordance with the microstructure of Fig. 2a.

3.2 Overall X-ray phase and texture analysis

The X-ray diffraction patterns recorded here, averaging the central areas of the specimens, cover reflections of ferrite, martensite and cementite. Additionally, weak-intensity reflections attributed to graphite were detected for the surface of the sword. Assuming the existence of these crystalline phases (Tab. 2), the experimental X-ray diffraction patterns were evaluated by means of the computer programme TOPAS (see sec. 2.4). Results of fitting the experimental diffraction patterns to calculated ones are expressed graphically in Fig. 6. The final reliability factors [30], other characteristics of refinement and the parameters of the crystalline phases are summarised in Tables 3 and 4 for the surface and cross-section of the blade, respectively. The quantitative results (Tables 3 and 4) as well as the X-ray diffraction patterns (Fig. 4) obtained for the surface and cross-section of the blade do not coincide in details. As already mentioned above, due to absorption limitations, only thin layers with a thickness of the order of magnitude of 10 μm contribute to the X-ray diffraction patterns. Thus, probably the difference observed reflects a real gradient of the characteristics of the crystalline phases present.

According to the results of Tables 3 and 4, approximately the same fraction of martensite (about 4.7 wt. %) is present near the surface and inside the blade, whereas the weight ratio of ferrite and cementite is different. It amounts to 73.3(8)/19.7(9) and 80.3(8)/15.0(8) for the surface and the interior, respectively. Additionally,

2.4(3) wt. % of free graphite was found at the surface. As to be estimated from the linear composition dependence of the ratio of unit cell parameters *c*/*a* (see [34], p. 491 and Tables 3 and 4), $Fe_{1-x}C_x$ martensite contains about 0.22 at. % and 0.26 at. % carbon at the surface and along the cross-section, respectively. Recalculation of element composition results in a carbon content for the surface and for the cross-section of the blade of about 2.8 wt. % and 1.5 wt. %, respectively. This might explain the striking difference of values for the average carbon content of 1.73 wt. % , 1.79 wt. % and 2.24 wt. % referred to in Table 1.

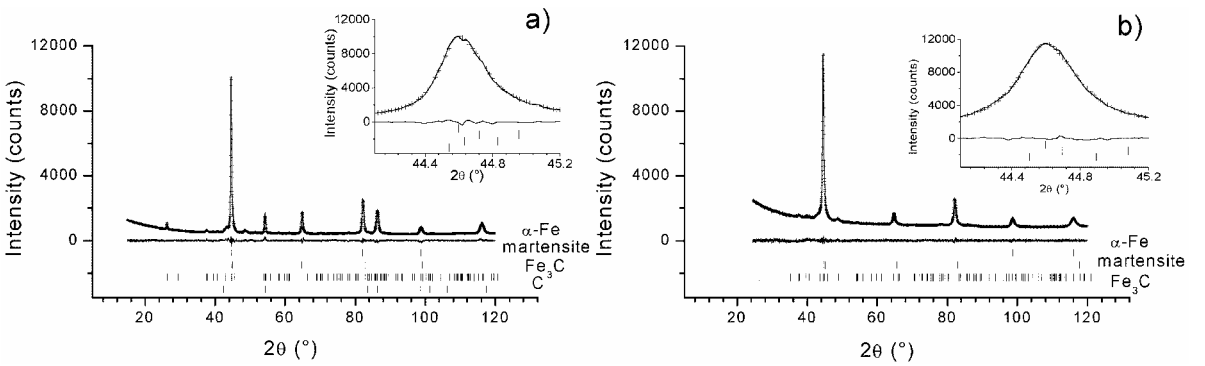

Fig. 6 Observed (solid line) and calculated (+) X-ray diffraction patterns (CuK_α radiation) of the blade surface (a) and cross-section (b). Using the final crystalline phase parameters, the diagram showing the difference between the observed and calculated pattern is displayed at the bottom of Figs. 4a and b. The bar diagrams below the powder pattern show the positions of symmetry-allowed reflections of the indicated crystalline phases used for fitting. To demonstrate the goodness of fit, the insets show both calculated and observed intensities for the most intensive reflections at higher magnification.

Table 3 Results of the refinement of specimen parameters from X-ray diffraction data recorded along the lateral face of the blade (R_{wp} = 5.25 %, R_p = 4.07 %, R_{exp} = 4.00 %, *GOF* = 1.31, Durbin-Watson statistics [36] parameter *DW* = 1.17, e.s.d. correction [37] factor = 2.6).

Phase Crystallite size (nm)	*a* (Å) *b* (Å) *c* (Å)	Texture direction 1 *r* [a] ratio	 direction 2 *r* [a] ratio	Phase content (wt. %)	B_{iso} (Å^{-2}) [b]	R_B (%)
α–Fe (ferrite)	2.87104(9)	[110]	[211]	73.3(8)	0.37(5)	0.90
243(39)	*a*	1.7(1)	0.3(1)			
	a	0.88(3)	0.12			
Fe_3C (cementite)	5.074(4)	[010]	[101]	19.7(9)	0.9(1)	3.14
7700 [f]	6.7563(4)	0.266(6)	0.51(6)			
	4.569(3)	0.77(2)	0.23			
$Fe_{1-x}C_x$ (martensite),	2.849(2)	[110]	[001]	4.6(9)	0.6 [f]	0.68
x = 0.002 [c]	*a*	0.70(9)	0.3(1)			
316 [f]	2.878(1)	0.62(6)	0.38			
C (graphite)	2.461(18)	[001]	-	2.4(3)	0.4 [f]	1.13
850 [f]	*a*	0.7(2)	-			
	6.756(3)	1.00	-			

[a] - parameter of March-Dollase texture [31]; [b] - general isotropic temperature factor of atoms; [c] - estimated from *c*/*a* ratio ([34], p. 491); [f] - fixed value

Determination of the volume fraction of cementite at the sword surface from line-counting analysis of Fig. 2 yielded 19.1 vol. % near the cutting edge, 18.5 vol. % in the middle and 18.6 vol. % near the back, corresponding to 18.3, 17.7 and 17.8 wt. % Fe_3C , respectively. The average value 17.9 wt. % Fe_3C is in a resonable agreement with the value 19.7(9) wt. % derived from X-ray phase analysis at the surface of the blade.

Comparison of the unit cell parameters of the crystalline phases given in Tables 2 , 3 and 4 shows that the real phases, especially ferrite and cementite near the surface, differ remarkably from the lattice parameters of

'pure' phases. Considering that most of the impurities listed in Table 1 are soluble at different levels in α-Fe maintaining the (average) W structure type, deviation of the lattice parameters is reasonable. Similarly, the carbide (cementite) – forming elements V, Mo, Cr, Mn, Nb and Co can substitute Fe atoms and, additionally, Si, S and B can substitute C atoms in the Fe_3C structure [28] giving rise to changes of the unit cell parameters of cementite. Gosh et al.[51] analysed the site occupancy of the metal substructure in cementite in the ortho- and paraequilibrium state for several transition metals using a thermodynamic and kinetic model. They found , for instance, that up to 27% of those sites were occupied by Co. In the case of coherent precipitates the resultant strain may give an additional contribution of both signs to changes of the lattice parameters (cf. [40]). Thus, the observed distortion of the unit cells of ferrite and cementite in our Damascus steel alloy can be understood.

Table 4 Results of the refinement of specimen parameters from X-ray diffraction data recorded along the cross-section of the blade (R_{wp} = 3.39 %, R_p = 2.67 %, R_{exp} = 2.84 %, *GOF* = 1.19, Durbin-Watson statistics [36] parameter DW = 1.76, e.s.d. correction [37] factor. = 1.5).

Phase Crystallite size (nm)	*a* (Å) *b* (Å) *c* (Å)	Texture Direction 1 *r* [a] ratio	 Direction 2 *r* [a] ratio	Phase content (wt. %)	B_{iso} (Å^{-2}) [b]	R_B (%)
α–Fe (ferrite)	2.87092(8)	[211]	-	80.3(8)	0.33(3)	0.20
243(29)	*a*	2.67(5)	-			
	a	1.00	-			
Fe_3C (cementite)	5.095(11)	-	-	15.0(8)	0.5(3)	0.47
800 [f]	6.757(9)	-	-			
	4.530(11)	-	-			
$Fe_{1-x}C_x$ (martensite), x = 0.003 [c]	2.842(7)	[001]	-	4.7(5)	0.6 [f]	0.15
395 [f]	*a*	0.49(3)	-			
	2.876(1)	1.00	-			

[a] - parameter of March-Dollase texture [31]; [b] - general isotropic temperature factor of atoms ; [c] - estimated from *c*/*a* ratio ([34], p. 491); [f] - fixed value

The X-ray diffraction patterns recorded from both, surface and cross-section of the sabre demonstrate a strong influence of texture of the crystalline grains present in the steel as expected from the microstructure analysis of sec 2.1. The texture effect is more pronounced in the case of the blade surface owing to the relative orientation of scan and banding directions (see also 3.1). Ferrite, martensite and cementite at the surface of the sword exhibited two directions of texture (Tab. 3). For cementite, these were the directions [010] and [101] as revealed from X-ray diffraction patterns of spatial zones far from the cutting edge (see Fe_3C reflections in Figs. 4 and 6 for comparison). Contrary to the surface, no texture was detected for cementite in the cross-section (Tab. 4) whereas the ferrite and martensite grains are characterised by only one direction of preferred orientation ([211] and [001], respectively) which is the minority at the sword surface, too.

3.3 High-resolution electron microscopy

In accordance with previous work quoted in ch. 1 and in agreement with our results of sec. 2.1, cementite is detected in the blade surface (i) as a component of the perlitic matrix and (ii) as large isolated grains arranged in bands with an average spacing of about 150 nm between them. Kochmann et al. [25] have given the first evidence of a third form of cementite in genuine Damascus steel, namely (iii) as nanowires. We present here additional data to confirm this finding. Fig.7(a) shows cross-sections of a number of Fe_3C wires piercing the plane of the picture. These cementite nanowires are mainly oriented parallel to each other in different areas of the specimen outside the cementite particles at a mutual distance of about 50 nm. However, these nanowires did not appear in all areas studied. Also, the preferred direction of the wires changed locally. Figs. 7(b) and 8 (a) are HRTEM images highlighting a characteristic stack of (100) and (010) lattice planes of the cementite structure, the projection of which is indicated in the structure model (Fig. 8 (b)). (010) planes are parallel to the wire axis. Slight changes of the orientation of the wire direction are accomplished by surface steps, so that the

wires are mostly monocrystalline. There are obvious similarities between the nanowires found here and the laminar cementite in pearlite. Zhou et al. [38] have shown that pearlitic cementite maintains the atomic habit plane (which is parallel to (010)) by microsteps during lamellar curvature (Note that [38- 41, 60] adopted the convention a < b < c for the order of the lattice parameter, whereas we stick to the convention c < a < b [28, 59]). Also, the orientation relationship betweeen cementite (c) and ferrite (f) or martensite in steel has been identified by various authors [38- 46, 56], whereby the relationship $(010)_c \parallel (011)_f$ found here matches that reported by [42, 46, 57,58]. We also want to point out that we found nanowires, the surrounding phase of which could not be identified unambiguously. Because the lattice spacings 2.88 , 3.03, and 4.62 Å occur , it may be monoclinic χ iron carbide Fe_5C_2 ((15) C 2/c –f^{3}e , mS28) reported by [61, 63]. Jack and Wild [63] pointed out that a close structural relationship exists between Fe_5C_2 and Fe_3C as indicated by the correspondence between two of the edge-lengths. This explains why in high-carbon martensitic steels ε iron carbide forming first [43] is replaced during tempering either by Fe_5C_2 or by Fe_3C. Any orientation relationship between a Fe_3C pecipitate and its matrix will have a closely corresponding relationship for the χ phase. Because several cementite nanowires were found surrounded by a matrix different from ferrite, martensite or austenite, which is probably the χ phase, then this may indicate just this transformation sequence.

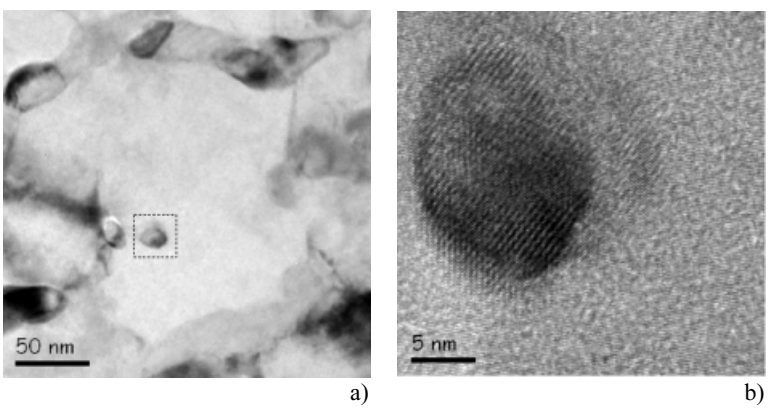

Fig. 7 HRTEM images of a Damascus blade showing cross-sections of several cementite nanowires (a) and one particular wire (b), which is marked by a dashed square in (a). The fringes leading upward from left to right in (b) correspond to lattice planes (100) with the lattice spacing d = 5.0 Å of Fe_3C. The matrix has been identified as Fe_5C_2 (fringes correspond to ($\bar{1}$01) planes).

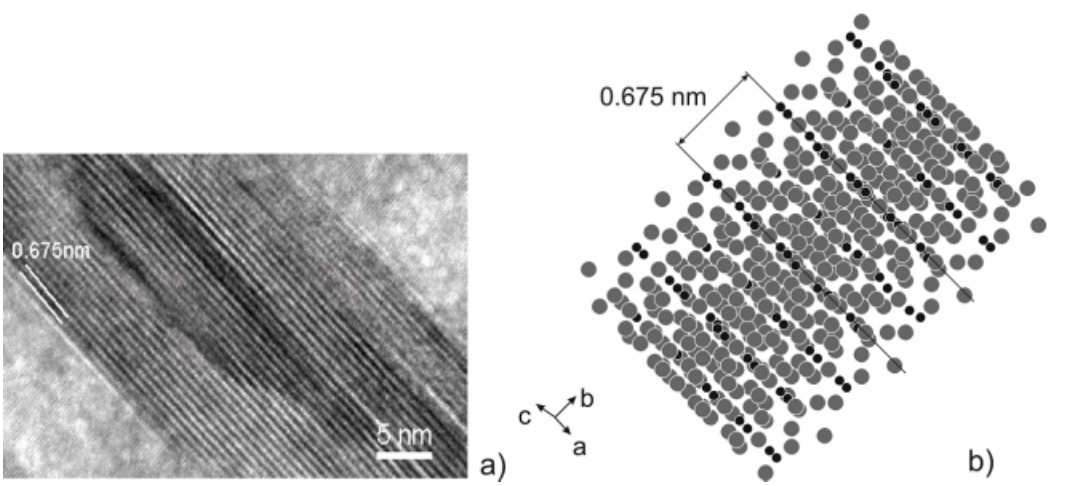

Fig. 8 HRTEM image of a Fe_3C nanowire (a). The fringes oriented along the longitudinal direction of the wire correspond to lattice planes. The lattice spacing d = 0.675 nm of (010) planes of the Fe_3C structure is indicated in the model projection (b) for comparison.

Fig. 8 displays more lattice planes used for the indentification of the wire structure, that support the proposed cementite structure.

While nanowires in Damascus blades have been observed for the first time, there were several previous indications of tiny precipitates in steels manufactured in the 20th/21st centuries which have diameters of the order of ~ 10-20 nm [51, 56, 62]. Also, very thin cementite lamellae in pearlite have been observed [38].

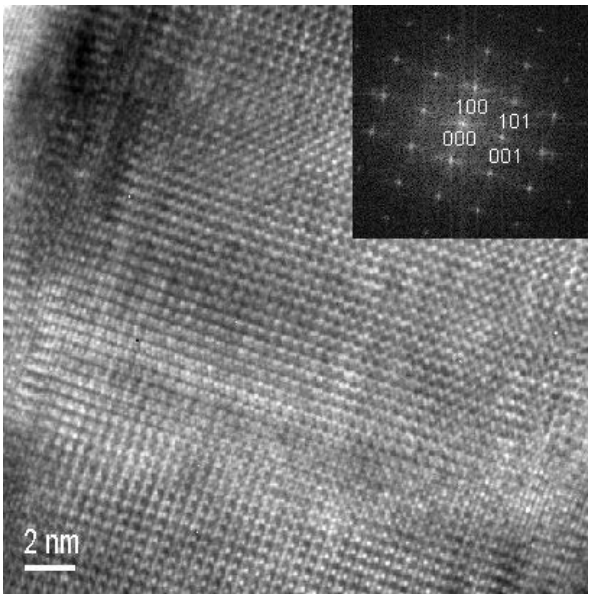

Fig. 9 HRTEM image of a Fe_3C nanowire in Damascus steel. The fringes correspond to various sets of lattice planes. The inset shows the Fourier transform of this image. Resultant reflections (d = 0.4434 nm, 0.3342 nm and 0.4900 nm) are indexed as Fe_3C 001, 101 and 100, respectively (the corresponding bulk spacings are d = 0.4520 nm, 0.3381 nm and 0.5100 nm).

3.4 Grain shape

The observation dealt with in sec. 3.3 is compatible with the [101] direction of texture found for about 23 % of the cementite at the blade surface (Tab. 3), although 3.3 refers to nanowires and the X-ray results are presumably governed by the micrometer scaled cementite. Probably, the preferred orientation of the main part (77 %) of cementite along [010] as registered by X-ray diffraction is caused by the texture of cementite grains. During fitting the X-ray diffraction patterns, the influence of texture was taken into account by a March-Dollase model (see 2.3) which can be used to describe both, plate- (texture parameter $r < 1$) and needle-like ($r > 1$) crystallites. As to be seen from results of refinement (Tables 3 and 4), only ferrite grains have texture parameter r characteristic of a needle-like shape. According to this analysis, crystalline grains of other phases are plate-like. In particular, a considerable degree of preferred orientation (r = 0.266) was found along the [010] direction of cementite grains at the blade's surface. The plate-like shape of crystalline grains of cementite as concluded from the results of fitting the X-ray diffraction patterns from the sabre's surface are in good agreement with results of microstructure studies (Fig.2). We observed that inside the blade large prolonged grains predominate, whereas at the surface of the sabre, bands appear to be formed by more rounded cementite grains. According to [19], the Fe_3C particles in the sabre under investigation are dominantly plate-like shaped with their broad face well aligned in the forging plane of the sabre blade.

The microstructure of the blade was found (cf.also [25]) consisting of a homogeneous fine-grained perlitic matrix with globular particle sizes down to several hundred nm and large planar bonds formed by cementite grains from 2 to 10 μm in diameter. These characteristic sizes of the crystallite grains are in reasonable agreement with the average crystallite sizes for ferrite and martensite (in the perlite matrix) and for cementite grains estimated by the Rietveld programme TOPAS (sec. 2.4, see Tables 3 and 4 for surface and cross-section of the blade).

3.5 New aspects of the microstructure

One interesting question with regard to the nanowires is certainly their nucleation. Following a proposal of Pitsch et al. [43], cementite might precipitate at (edge) dislocations in ferrite, which are attracting carbon. Since dislocation lines prefer certain lattice directions and slip planes, an orientation preference may occur. Depending on that orientation, an orientation relationship cementite/ferrite occurs. Moreover, impurity elements may facilitate both the nucleation (in particular V [5,49]) and the growth kinetics [51].

Another aspect refers to the role of magnetic properties of cementite. It is ferromagnetically ordered with a Curie temperature of $T_c \approx 210$ °C [52,53]. Using neutron diffraction, Wood et al. [53] concluded that the magnetization of cementite is parallel to [100]. The magnetic ordering temperature of ferrite is much higher (~770 °C) so that during forging the matrix may be magnetically ordered whereas the nanowires are not. At

ambient temperatures, according to the orientation relationship found in sect 3.3., the direction of magnetisation of the cementite wires may be parallel to the wire axis as well as to the soft direction [100] of iron.

4 Conclusions

The sabre displayed markedly parallel alignment of the cementite sheets over fairly long distances with an average spacing of 50-60 μm. As an important outcome of our investigation the distribution of cementite - contrary to that of ferrite and martensite - at the surface of the sword was found to be inhomogeneous. Cementite content was detected firstly in regions about 6 mm distant from the cutting edge of the sword reaching a maximum near its back. Additionally, near the cutting edge of the sword the hexagonal modification trydimite of SiO_2 was found. The presence of trydimite as well as hints to the χ-phase and to an unknown phase in this area can be explained by peculiarities of the processing of the surface (inclusive later grinding). This can apply also to the small content of free graphite (2.4(3) wt. %), which was found at the entire surface.

When scanning the phase content along the cross-section perpendicular to the cementite bands no inhomogeneity was detected. Approximately the same volume of martensite of about 4.7 wt. % is present at the surface and in cross-section of the blade whereas the weight ratio of ferrite and cementite was found to be 73.3(8)/19.7(9) and 80.3(8)/15.0(8), respectively.

Using the code TOPAS we succeeded in evaluating the texture of this fine-grained steel. The texture is more pronounced along the blade surface. Ferrite, martensite and cementite exhibited at the surface two directions of texture. For cementite, these were the directions [010] and [101]. Unlike the surface of the sabre, no texture was detected for cementite in the cross-section whereas the ferrite and martensite grains are characterised by only one direction of preferred orientation ([211] and [001], respectively). Ferrite grains exhibit a needle-like shape while other phases show rather a plate like habitus.

Employing HRTEM analysis further evidence has been supplied for the structure of nanowires and the phases surrounding them.

Acknowledgements Authors gratefully acknowledge the help of Ms. Thurid Stephan and Ms. Heide Müller.

References

[1] J. Panseri, Gladius **4**, 5 (1965)
[2] J. Wadsworth and O. D. Sherby, Prog. Mater. Sci. **25**, 35 (1980).
[3] C. S. Smith, A History of Metallography, (1988) The MIT Press, Cambridge, Mass.
[4] M. Sachse, Damaszener Stahl, (1993) Verlag Stahleisen, Düsseldorf.
[5] J. D. Verhoeven, Sci. Amer. **284**, 74 (2001).
[6] P. Anoçoff, Gornyj Journal **1**, 162 (1841).
P. Anoçoff, Annuaire du Journal des Mines de Russie **192** (1841).
[7] N. Belaiew and O. Bulatach, St. Petersburg (1906).
[8] N. Belaiew, Metallurgie **8**, 57 (1911).
N. Belaiew, Metallurgie **8**, 493 (1911).
[9] N. Belaiew, J. Iron Steel Inst. **97**, 417 (1918).
[10] N. Belaiew, J. Iron Steel Inst. **104**,181 (1921).
[11] A. Sauveur, The Metallography and Heat Treatment of Iron and Steel, 208 (1910) Cambridge, Mass.
[12] B. Zschokke, Rev. de Métallurgie **21**, 635 (1924).
[13] K. Harnecker, Stahl u. Eisen **44**,1409 (1924).
[14] R. Zeller, Jahrbuch des Bernischen Historischen Museums **4**, 24 (1924).
[15] J. Piaskowski, J. Hist. Arabic Sci. **2**, 3 (1978).
[16] J. D. Verhoeven, H. H. Baker, D. T. Peterson, H. F. Clark, and W. M. Yater, Mater. Char. **24**, 205 (1990).
[17] D. T. Peterson, H. H. Baker, and J. D. Verhoeven, Mater. Char. **24**, 355 (1990).
[18] J. D. Verhoeven and A. H. Pendray, Mater. Char. **29**, 195 (1992).
[19] J. D. Verhoeven, A. H. Pendray, and W. E. Dauksch, JOM **50**, 58 (1998).
[20] J. Wadsworth and O. D. Sherby, Mater. Char. **28**, 165 (1992).
[21] J. Wadsworth, MRS Bulletin **27**, 980 (2002).
[22] J. D. Verhoeven and L. L. Jones, Metallography **20**, 153 (1987).
[23] J. D. Verhoeven, A. H. Pendray, and E. D. Gibson, Mater. Char. **37**, 9 (1996).
[24] O. D. Sherby and J. Wadsworth, SAMPE Journal **31**, 10 (1995).

[25] W. Kochmann, M. Reibold, R. Goldberg, W. Hauffe, A. A. Levin, D. C. Meyer, T. Stephan, H. Müller, A. Belger, and P. Paufler, J. Alloys & Comp. **372**, L15 (2004).
[26] Letter by E. J. Kläy dated 20 June 1996. Personal communication of W. Kochmann.
[27] TOPAS. General profile and structure analysis software for powder diffraction data. Version 2. 0, Bruker AXS GmbH, Germany (2000).
[28] P. Villars and L. D. Calvert, Pearson's Handbook of Crystallographic Data for Intermetallic Phases, 2nd ed., vols. 1-4, American Society for Metals, Metals Park, Ohio (1991).
[29] A. J. C. Wilson (ed.), International Tables for Crystallography, Vol. C, Kluwer Academic Publishers, Dordrecht/ Boston/ London (1992).
[30] R. E. Young (ed.), The Rietveld Method, Oxford University Press, New York (1995).
[31] W. A. Dollase, J. Appl. Cryst. **19**, 267 (1986).
[32] J.-F. Bérar and P. Lelann, J. Appl. Cryst. **24**, 1 (1991).
[33] M. Reibold, A. A. Levin, D. C. Meyer, N. Pätzke, and P. Paufler to be published
[34] H. Schumann, Metallographie, 13Aufl., Deutscher Verl. f. Grundstoffind., Leipzig (1991).
[35] J. E. Fleming and H. Linton, Phys. Chem. Glasses **1**, 148 (1960); ICSD card 29343.
[36] R. J. Hill and H. D. Flack, J. Appl. Cryst. **20**, 356 (1987).
[37] J. -F. Bérar and P. Lelann, J. Appl. Cryst. **24**, 1 (1991).
[38] D. S. Zhou and G. J. Shiflet, Metallurg. Trans. **23A**, 1259 (1992).
[39] I. V. Isajčev, Ž. Techn. Fiziki **17**, 835 (1947).
[40] Ju. A. Bagarjackij, Doklady Akad. Nauk SSSR **73**, 1161 (1950).
[41] J. J. Trillat and S. Oketani, Acta Cryst. **5**, 469 (1952).
[42] N. J. Petch, Acta Cryst. **6**, 96 (1953).
[43] W. Pitsch and A. Schrader, Archiv f. d. Eisenhüttenwesen **29**, 715 (1958).
[44] W. Pitsch, Acta Metall. **10**, 79 (1962).
[45] P. B. Boswell and G. A. Chadwick, Scripta Met. **11**, 1001 (1977).
[46] K. H. Liu, H. Chan, M. R. Notis, and V. C. Pigott, In: Microbeam Analysis 1984 (ed. By A. D. Romig Jr., J. I. Goldstein), San Francisco Press, p. 261 (1984).
[47] Hysitron Inc., http://www. hysitron. com/Applications/Multiphase%20materials. htm.
[48] D. Tabor, The hardness of metals. Clarendon Press, Oxford (1951), p. 164.
[49] H. Han, D. V. Edmonds, and G. D. W. Smith, Metallurg. Mater. Trans. **32A**, 1313 (2001).
[50] C. T. Liu and J. Gurland, Trans. Metallurg. Soc. AIME **242**, 1535 (1968).
[51] G. Gosh and G. B. Olson, Acta Materialia **50**, 2099 (2002).
[52] S. W. J. Smith, W. White, and S. G. Barker, Proc. Phys. Soc. London **23**, 61 (1911).
[53] A. Tsuzuki, S. Sago, S. Hirano, and S. Naka, J. Mater. Sci. **19**, 2513 (1984).
[54] I. G. Wood, L. Vočadlo, K. S. Knight, D. P. Dobson, W. G. Marshall, G. D. Price, and J. Brodholt, J. Appl. Cryst. **37**, 82 (2004).
[55] S. Fedosov, Proc. of Int. Conf. "Technology 99", STU Bratislava, 8-9 Sept. 1999, v. 1, p. 50-52.
[56] G. D. Suchomlin, Fizika Metallov i Metallovedenie **42**, 965 (1976).
[57] I. V. Isajčev, Ž. Techn. Fiziki **17**, 839 (1947).
[58] M. Arbusov and G. Kurdjumov, Ž. Techn. Fiziki **11**, 412 (1941).
[59] F. H. Herbstein and J. Smuts, Acta Cryst. **17**, 1331 (1964).
[60] S. B. Hendricks, Z. Krist. **74**, 534 (1930).
[61] K. -H. Jack and S. Wild, Nature **212**, 248 (1966).
[62] X. Huang and N. H. Pryds, Acta mater. **48**, 4073 (2000).
[63] M. J. Duggin and L. J. E. Hofer, Nature **212**, 248 (1966).